Development of Therapeutic Au–Methylene Blue Nanoparticles for Targeted Photodynamic Therapy of Cervical Cancer Cells

ARTICLE *in* ACS APPLIED MATERIALS & INTERFACES · DECEMBER 2014

Impact Factor: 6.72 · DOI: 10.1021/am5064298 · Source: PubMed

4 AUTHORS, INCLUDING:

Jiashing Yu
National Taiwan University
42 PUBLICATIONS **587** CITATIONS
SEE PROFILE

Chih-Chia Huang
National Cheng Kung University
47 PUBLICATIONS **1,072** CITATIONS
SEE PROFILE

Po-Yang Chang
National Yang Ming University
3 PUBLICATIONS **4** CITATIONS
SEE PROFILE

ACS APPLIED MATERIALS & INTERFACES

Research Article

www.acsami.org

Development of Therapeutic Au–Methylene Blue Nanoparticles for Targeted Photodynamic Therapy of Cervical Cancer Cells

Jiashing Yu,*[,†,⊥] Che-Hao Hsu,[†,⊥] Chih-Chia Huang,*[,‡,§,⊥] and Po-Yang Chang[‡]

[†]Department of Chemical Engineering, National Taiwan University, Taipei 106, Taiwan

[‡]Institute of Biophotonics, National Yang-Ming University, Taipei 112, Taiwan

[§]Biophotonics and Molecular Imaging Research Center (BMIRC), National Yang-Ming University, Taipei 112, Taiwan

Supporting Information

ABSTRACT: Photodynamic therapy (PDT) involves the cellular uptake of a photosensitizer (PS) combined with oxygen molecules and light at a specific wavelength to be able to trigger cancer cell death via the apoptosis pathway, which is less harmful and has less inflammatory side effect than necrosis. However, the traditional PDT treatment has two main deficiencies: the dark toxicity of the PS and the poor selectivity of the cellular uptake of PS between the target cells and normal tissues. In this work, methylene blue (MB), a known effective PS, combined with Au nanoparticles (NPs) was prepared using an intermolecular interaction between a polystyrene-*alt*-maleic acid (PSMA) layer on the Au NPs and MB. The Au@polymer/MB NPs produced a high quantum yield of singlet oxygen molecules, over 50% as much as that of free MB, when they were excited by a dark red light source at 660 nm, but without significant dark toxicity. Furthermore, transferrin (Tf) was conjugated on the Au@polymer/MB NPs via an EDC/NHS reaction to enhance the selectivity to HeLa cells compared to 3T3 fibroblasts. With a hand-held single laser treatment (32 mW/cm) for 4 min, the new Au@polymer/MB-Tf NPs showed a 2-fold enhancement of PDT efficiency toward HeLa cells over the use of free MB at 4 times dosage. Cellular staining examinations showed that the HeLa cells reacted with Au@polymer/MB-Tf NPs and the 660 nm light excitation triggered PDT, which caused the cells to undergo apoptosis ("programmed" cell death). We propose that applying this therapeutic Au@polymer/MB-Tf nanoagent is facile and safe for delivery and cancer cell targeting to simultaneously minimize side effects and accomplish a significant enhancement in photodynamic therapeutic efficiency toward next-generation nanomedicine development.

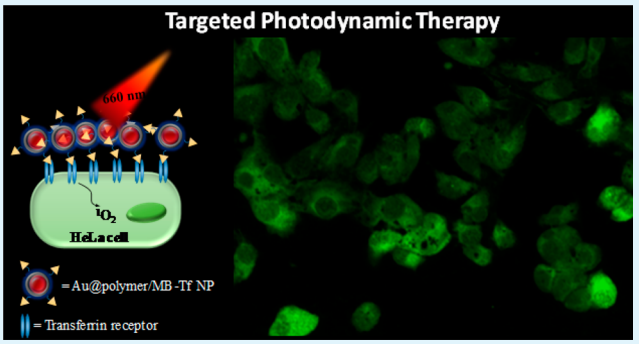

KEYWORDS: *gold@polymer, nanoparticles, methylene blue, transferrin, photodynamic therapy*

1. INTRODUCTION

Photodynamic therapy (PDT), which combines a light source, oxygen molecules, and a photosensitizer (PS) to generate reactive oxygen species (ROS), has been widely researched and proven effective for treating different types of cancer.[1−3] ROS would also be generated in the presence of reducing agents, which consist of type II and type I reactions.[4−6] However, traditional PDT treatment cannot usually be applied to a region that is deep within the body due to the limitations of the light source penetration. The selective delivery of PS to the targeted area of the tumor site was also a problem and requires efficient accumulation in cancer cells in order to prevent random distribution in the skin tissue from causing light-induced superficial skin lesions.[7,8] In addition, the dark toxicity of several PS compounds increases with the dose and incubation time.

The methylene blue molecule is a member of the phenothiazinium family and is a PS with excellent photochemical properties for generating high quantum intersystem crossing ($\Phi_T \sim 0.52$) of singlet oxygen, showing potential as a PS candidate for PDT. It has been reported that MB has been clinically used for the treatments of basal cell carcinoma, Kaposi's sarcoma, melanoma, and virus and fungal infections.[4] In addition to MB's appealing photochemical properties, its excitation at a pure dark red wavelength (650−670 nm) within the "optical window"[9,10] can decrease endogenous absorption of water and pigments in the biological environment and is also advantageous for PDT applications. Typically, the cytotoxic ROS generated by MB and PDT treatments often trigger cell death, which is a moderate therapeutic method of cancer tumor elimination.[11−13] Apoptosis ("programmed" cell death) is less harmful than necrosis.[14] Moreover, MB costs only ~$2 USD/g and is an inexpensive chemical when compared to other commercially available photosensitizers in clinical use, for

Received: September 18, 2014
Accepted: December 10, 2014

   dx.doi.org/10.1021/am5064298 | ACS Appl. Mater. Interfaces XXXX, XXX, XXX−XXX

example over $10 000 for Photofrin, Verteporfin, protoporphyrin-based PDT drugs, and [Ir(dtbbpy)(ppy)2][PF6]. In spite of these advantages, dark cytotoxicity occurs in doses of MB over 20 μM.[11−13] This is because MB easily crosses the cell membrane with the aid of its benzene ring structure and accumulates in mitochondria, lysosomes and double-stranded DNA.[6,11−13] To improve these aforementioned shortcomings, we designed the Au@polymer nanostructure encapsulated with MB drug to prevent leakage of MB molecule and cause collateral damage to cellular organelles. When conjugated with transferrin (Tf) protein, an enhancement in the targeted PDT treatment would be accessed through transferrin receptor-mediated endocytosis pathway, rather than slow diffusion of MB into cells. Au@polymer core−shell NPs were prepared by our previous one-pot polymerization shell coating method[15] following tightly and physically bonding methylene blue (MB) PSs and functionalization with transferrin (Tf) proteins, leading to the formation of a sandwich structure, as shown in Figure 1.

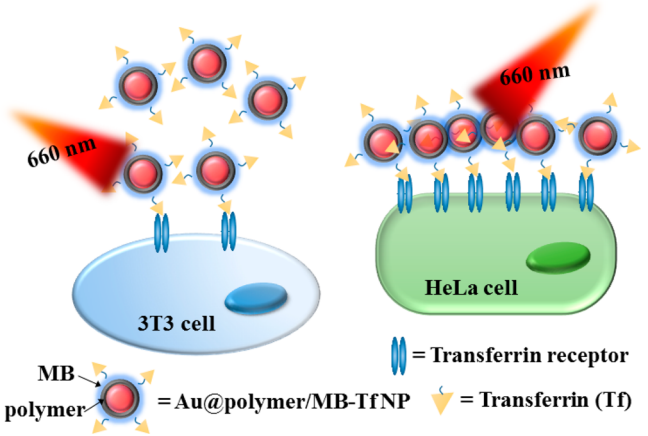

Figure 1. Schematic illustration of the preparation of Au@polymer/MB-Tf NPs and their application for targeted PDT treatment for killing HeLa cancer cells with a 660 nm light excitation.

Our demonstration showed that the Au@polymer/MB-Tf NPs could enhance the Tf receptor (TfR) targeting selectivity of HeLa cells (human cervical cancer cell line) compared to 3T3 fibroblasts and thus eliminate HeLa cancer cells effectively with fewer side effects when applied in PDT treatment.

In recent years, nanoparticles (NPs) have received much attention in many fields, including biomedical applications. Because of their small size and relatively high surface area-to-volume ratio, NPs have unique and desirable properties.[15−18] In addition, NPs have a longer half-life in the body's circulatory system, known enhanced permeability and retention effects in nanoscale particles,[19] and can easily enter the cell body due to their particles size effect.[20] Many types of NPs have been researched for biomedical use, such as quantum dots, magnetic NPs, polymer NPs, and metal polymers.[21−24] Among the many NPs for biomedical use, Au nanomaterials have shown great potential in cell tracking, drug delivery, photothermal therapy, and molecular imaging.[25−29] Au NPs are chemically inert, nontoxic, and easy to modify.[15,19,20,26−29] Therefore, Au NPs are easily combinable with other materials to develop a multifunctional and biocompatible drug delivery nanocarrier. Research on gold nanoparticle−MB composites in recent years has focused primarily on their applications in molecular imaging and catalysis. With the aid of surface-enhanced Raman scattering (SERS) and other electrochemical techniques, the spatial distribution of methylene blue in gold nanoparticle−MB composite has been investigated.[30] Studies of biosynthesized gold and silver nanoparticle cataylized degradation of MB were also performed.[31] However, investigation into the application of gold nanoparticle-MB NPs in targeted delivery and PDT has rarely been studied. For PDT applications, Khan et al. utilized gold nanoparticle-MB NPs for inhibiting the growth of a *Candida albicans* biofilm throught a PDT reaction after excitation at 660 nm.[32] This study did not provide evidence of the photochemical properties of phototoxicity by ROS and was not a targeted effort for the PDT treatment. In this work, we utilized 9,10-anthracenediyl-bis (methylene)dimalonic acid indicator by using UV−visible spectra and single oxygen emission at ∼1270 nm with a fluorescence spectrometer to prove the type II phototoxicity from the Au@polymer/MB NPs after excitation at 660 nm. The Au@polymer/MB NPs have similar quantum yields (QYs) of singlet oxygen production as that produced by free MB molecules, but performed more effectively with the selective PDT elimination of HeLa cancer cells.

2. RESULTS AND DISCUSSION

2.1. Characterization of Au NPs. To prevent the close contact of MB and Au NP from causing nonradiative energy transformation[33,34] and possibly depleting the yields of singlet oxygen molecules, a spacer composed of a polystyrene-*alt*-maleic acid (PSMA) polymer layer was designed to prepare the Au@polymer NPs first. The MB solution was added to the surface of the Au NPs via $\pi-\pi$ stacking and/or electrostatic interactions.[15] By possibly decreasing the release of the PS and locally concentrating the effect of the Au@polymer/MB NPs, we hypothesized that this development of a novel drug delivery platform could simultaneously reduce the MB's dark toxicity and enhance the PDT efficiency.

The Au@polymer NPs were synthesized via a hydrothermal reaction of poly(styrene-*alt*-maleic acid)sodium salt, 13 wt % solution in water (5.45 g/mL), and $HAuCl_4$ solution (4.45 mM) in accordance with our previous synthesis method.[15] After 6 h of reaction time, each spherical Au NPs (∼21 nm) was decorated with a thin PSMA layer (Figure 2a). The collected sample concentration was estimated to be 489.3 ± 77.5 $ppm_{[Au]}$ according to atomic absorption spectroscopy (AAS) measurements. On the basis of the XRD pattern, we concluded that the Au in the center of the Au@polymer NPs was in element form with a face-centered cubic structure (Figure 2b). Owing to the carboxylate structure of the PSMA polymer, the surface charge of the Au@polymer NPs showed a ζ-potential of −44.8 mV (Table S1, Supporting Information), which is advantageous for the subsequent absorption of positively charged MB molecules.

2.2. Optical Properties of Au@polymer and Au@polymer/MB NPs. Next, we utilized a UV−visible spectrometer to analyze the concentration-dependent absorption of MB molecules at the polymer surface of the Au@polymer NPs (Figure 2c). After the interaction of Au@polymer NPs (50 ppm) with 0−22 μM of MB solution, Au@polymer/MB NPs were obtained. These nanoproducts showed three absorption peaks located at ∼540, 610, and 660 nm. The first is very large and could be assigned to a surface plasmon resonance (SPR) band of Au NPs. In addition, the absorption peak at approximately 660 nm was determined to be due to a monomer form of the MB molecule[35] that resided on the

dx.doi.org/10.1021/am5064298 | ACS Appl. Mater. Interfaces XXXX, XXX, XXX−XXX

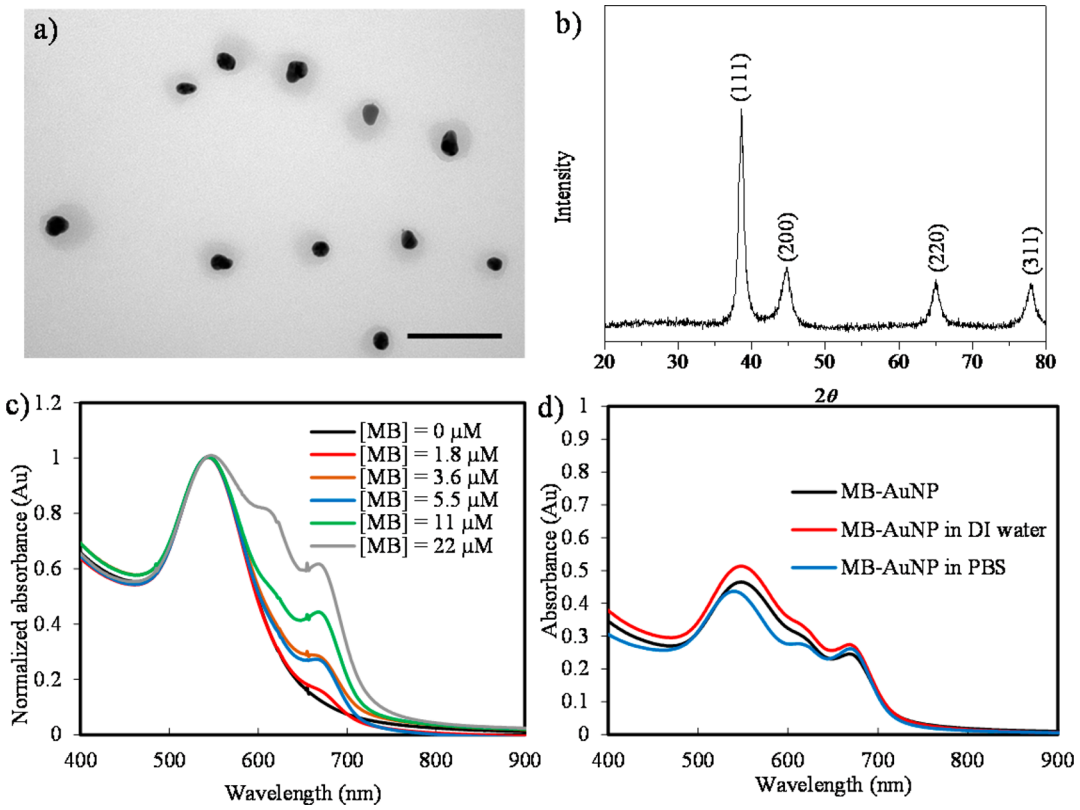

Figure 2. (a) TEM image and (b) XRD pattern of the Au@polymer NPs (scale bar: 100 nm). (c) UV−visible spectra of Au@polymer NPs reacted with 0−22 μM of MB concentrations and (d) MB (22 μM)-loaded Au@polymer NPs dispersed in deionized water and PBS solutions before and after 14 days.

polymer shell, whereas a shoulder developed at approximately 610 nm for the MB dimer structure as the MB concentrations increased significantly, from 11 μM to 22 μM. The amount of MB adsorption on the Au@polymer NPs as a function of the addition of MB concentration was plotted in Figure S1 (Supporting Information). For an MB concentration range from 5.5 to 22 μM, the MB PS was not detectable in the supernatant after centrifugation of the Au@polymer/MB samples solution, and the graph was almost linear. An average of 29 490 MB molecules was attached to single Au@polymer NPs according to the quantification of 22 μM of MB PSs loaded into ~50 $ppm_{[Au]}$ of Au@polymer NP solution. However, as the MB concentration approached 36.4 μM, the graph plateaued, which was probably due to the saturated adsorption amount. It was noted that the preparation of Au@polymer/MB NPs with 36.4 μM resulted in the formation of particle aggregates (Figure S2a, Supporting Information) and absorption band shifting (Figure S2b, Supporting Information). To prepare stable Au@polymer/MB NPs and carry a maximum amount of MB, 22 μM MB PS attached to the surface of Au@polymer NPs was determined to be the optimal condition under saturation absorption for the cellular studies and photodynamic therapy.

2.3. Stability Test of Au@polymer/MB NPs. In the stability test, an Au@polymer/MB NP solution at 22 $\mu M_{[MB]}$ and ~50 $ppm_{[Au]}$ concentration was used for optical analysis. The cumulative amounts of MB released at each time point were quantified. When compared to the original MB loading amount, the MB leakage after 14 days was negligible (Figure S3, Supporting Information). Moreover, the UV/visible spectra of Au@polymer/MB NPs in phosphate buffered saline (PBS) and deionized (DI) water solution showed that a single SPR peak from the Au@polymer NPs at 540 nm accompanied by double absorption bands (at 610 and 660 nm), due to the stable resident MB, was still retained after 14 days (Figure 2d). Results showed that the Au@polymer/MB NPs are quite stable in both DI water and PBS buffer solution, indicating that the Au@polymer NPs are a good carrier and not only bind to MB tightly but also retain the optical properties of MB that could be applied to further PDT treatment.

2.4. ROS Generation Test: ABDA Method. To detect ROS generated from MB-based Au@polymer NPs during the exposure to a 660 nm laser (75 mW) for 4−30 min, 9,10-anthracenediyl-bis(methylene)dimalonic acid (ABDA) was used. ABDA has three strong absorption peaks at 360, 380, and 400 nm. In the presence of singlet oxygen or ROS, ABDA rapidly reacts with ROS, followed by a decrease of all three peaks.[36,37] In this experiment, a series of as-prepared Au@polymer/MB NPs was prepared at 50 $ppm_{[Au]}$ with MB concentrations of 11 and 22 μM. Au@polymer NPs alone and free MB with the same concentrations as above were used. Results from the Au@polymer/MB NPs groups showed that the ability to generate ROS is dose dependent on the MB concentration, whereas the pure Au@polymer NPs group showed negligible ROS production (Figure 3a). When compared with the free MB groups, the Au@polymer/MB NPs showed a stable and continuous increase in the generation of ROS. It has been reported that monomer species of MB favor a high type II yield of singlet oxygen.[4] The domination of dimer forms in the high free MB concentration resulted in the decrease of the MB monomer amount. We carried out a low sample dose (12.5 $ppm_{[Au]}$ with MB concentrations of 2.7 and

dx.doi.org/10.1021/am5064298 | ACS Appl. Mater. Interfaces XXXX, XXX, XXX−XXX

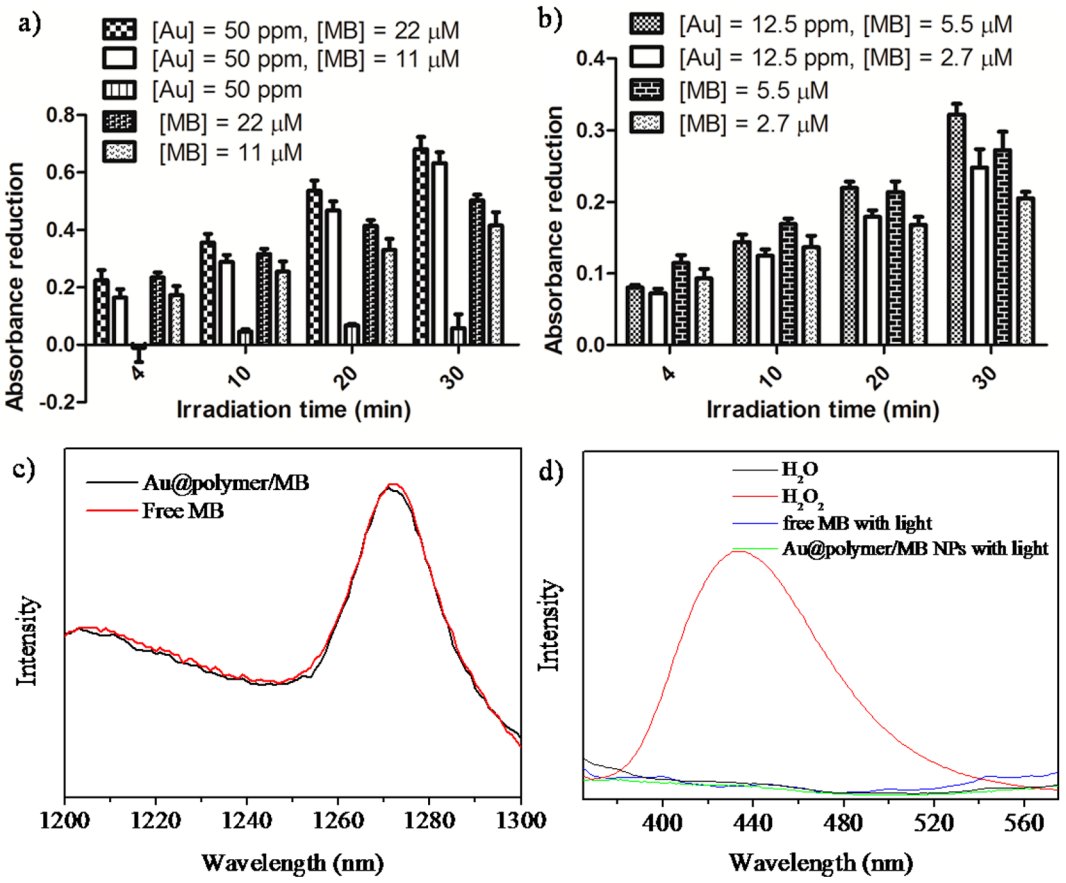

Figure 3. ABDA absorbance reduction at 400 nm for (a) high and (b) low sample concentrations of the free MB and Au@polymer/MB NPs as a function of irradiation time. [Au] represents the concentration of the Au@polymer/MB NPs in the solution, whereas [MB] represents the final concentration of MB in the solution. Data are presented as mean ± standard deviation (n = 3). (c) Fluorescence spectra of the generation of single oxygen molecules from free MB (2.2 μM) and Au@polymer/MB NPs (5 $ppm_{[Au]}$ and 2.2 μM) upon 660 nm light excitation (75 mW). (d) Fluorescence spectra of the aqueous solution include TA only (black line); TA and H_2O_2 (1 mM) (red line); TA and MB (11 μM) with 660 nm laser (75 mW) (blue line); TA and Au@polymer/MB NPs (25 $ppm_{[Au]}$ and 11 μM) with 660 nm laser (75 mW) (green line). The concentration of TA was 0.5 mM.

5.5 μM), as shown in Figure 3b. There is no significant difference between the Au@polymer/MB NPs and free MB molecules at a short irradiation time. Indeed, the QY of singlet oxygen molecule generation was nearly identical for both the Au@polymer/MB NPs and free MB molecules (~50% of QY), according to the similar fluorescence intensity the from $^1O_2$ molecules at 1270 nm (Figure 3c), which indicate the absence of nonradiative energy transformation.

Considering the possible production by other ROS species, we performed the additional examination to monitor the generation of hydroxyl radical (·OH) from the Au@polymer/MB NPs and free MB molecules after laser excitation at 660 nm. Terephthalic acid (TA) was used as a molecular probe to detect ·OH by the conversion of TA to fluorescent 2-hydroxyterephthalic acid (TAOH). As reaction TA with H_2O_2 molecules, which could slowly decompose into ·OH radicals and hydroxide ions, the generation of emission at around 435 nm was detectable (Figure 2d). However, there is no remarkable fluorescence from the H_2O, Au@polymer/MB NPs, and free MB molecules after 4 min of irradiation time, indicating the absence of ·OH radicals via Type I mechanism.

Au@polymer/MB NPs were rugged and had a remarkable yield of ROS after 30 min of irradiation. This is probably due to the Au@polymer/MB NPs resistance to the photobleaching of the MB molecules during exposure to a laser light. To support these speculations, a 660 nm light excitation of Au@polymer/MB NPs during 0−8 min possessed a stable MB molecular absorption band (Figure S4, Supporting Information), in contrast to pure MB. These results indicated that that the Au@polymer/MB NPs retained the ability to generating ROS, which is important for PDT treatment.

2.5. In Vitro Cell Toxicity Test. A cell toxicity test using a series of as-prepared Au@polymer/MB NPs was prepared at 50 ppm $_{[Au]}$ (with MB concentrations of 11 and 22 μM) and at 12.5 ppm $_{[Au]}$ (with MB concentrations of 2.7 and 5.5 μM) and was reacted on HeLa cells. After 2 h of incubation, the cells were exposed to a 660 nm light excitation for 4 min and then returned to an incubator for another 24 h of culture. Cell viability was plotted with the concentration of MB in the culture medium (Figure 4). Both the PDT treatment efficiency and dark toxicity are dose dependent. The pure Au@polymer NPs showed their biocompatibility. In comparison with pure MB groups for 67% at 2.7 μM and 63% at 5.5 μM, 12.5 $ppm_{[Au]}$ of Au@polymer/MB NPs effectively reduces dark toxicity over 97% of cell variability at 2.7 and 5.5 μM concentrations of MB. It is important to note that when [Au] is at 50 ppm and [MB] is at 22 μM, the cell viability was slightly reduced to 77% without laser excitation, probably due to excessive MB-based particle accumulation in cell organelles. The Au@polymer that carried MB molecules readily reduced the dark toxicity of MB

dx.doi.org/10.1021/am5064298 | ACS Appl. Mater. Interfaces XXXX, XXX, XXX−XXX

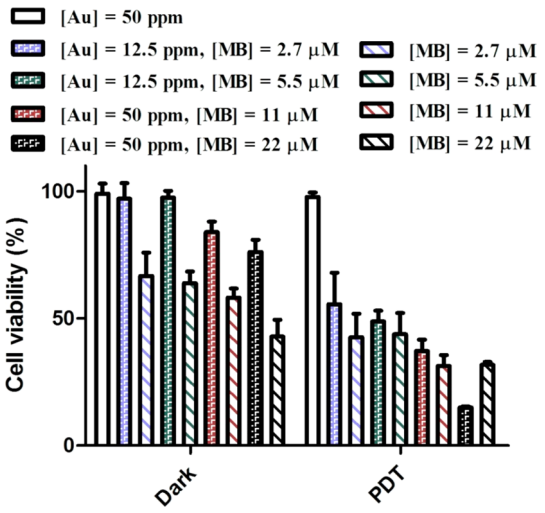

Figure 4. Cell viability (with MTT assay) of HeLa cells incubated with Au@polymer/MB NPs and MB alone for 2 h and then treated with two conditions of 660 nm light excitation for 4 min and dark aging (4 min) followed by an another incubation for 24 h. [Au] represents the concentration of the Au@polymer NPs in a cell culture medium, whereas [MB] represents the final concentration of MB in a cell culture medium. Data are presented as mean ± standard deviation (n = 3).

but retained nearly the same PDT efficiency as pure MB when [Au] was at 12.5 ppm and [MB] was at 5.5 μM. A similar trend of less dark toxicity and compatible phototoxicity on HeLa, A549, and HT1080 cells also observed when incubated with Au@polymer/MB NPs, compared to cells treated with free MB (Figure S5, Supporting Information). Therefore, we used these conditions in the following experiments.

2.6. Transferrin Conjugation onto Au@polymer/MB NPs. Past investigations have established that the Tf-targeted delivery of anticancer drugs into different cancer cell lines presented with 3- to 10-fold more cytotoxicity than drugs alone.[38] A receptor-mediated endocytosis pathway was proposed to increase the cellular uptake and internalization of therapeutic agents. By using the carboxylate group on the polymer surface, transferrin (Tf) was conjugated to Au@polymer NPs via an EDC/NHS reaction. The excess Tf was quantified by using a BCA assay (Figure S6, Supporting Information). An average of 153 ± 19 Tf was estimated to conjugate to a single Au@polymer NP. After the surface modification of Tf, the surface charge of the Au@polymer-Tf NPs drastically increased to a ζ-potential of −37.3 mV from −44.8 mV with the Au@polymer NPs (Table S1, Supporting Information), implying a successful bioconjugation. The absorption of the MB molecule on the Au@polymer-Tf NPs was prepared with the same methods described above to reach saturation absorption. The loading amount of MB on the Au@polymer-Tf NPs was found to be nearly the same as the Au@polymer/MB NPs (~50 $ppm_{[Au]}$ and ~20 $\mu M_{[MB]}$). Figure S7 (Supporting Information) shows that the Au@polymer/MB-Tf NPs presented similar optical properties as the Au@polymer/MB NPs. A slight decrease in the surface charge for the Au@polymer/MB-Tf NPs (−30.3 mV) was obtained (Table S1, Supporting Information) after an absorption of positively charged MB molecules, suggesting a screening of the negatively charged carboxylate group on the polymer surface.

2.7. Cellular Interaction Quantification. To compare the cell targeting selectivity between cancer cells and nonmalignant cells, HeLa cells and 3T3 fibroblasts were used. After incubation with the Au@polymer-Tf NPs and Au@polymer NPs (12.5 ppm) for 24 h, the binding interaction between cell membrane proteins and particles was measured by atomic absorption spectroscopy (AAS) measurement. After 2 h of incubation, the selectivity of the Au@polymer-Tf NPs and Au@polymer NPs to cells was plotted (Figure 5a). The

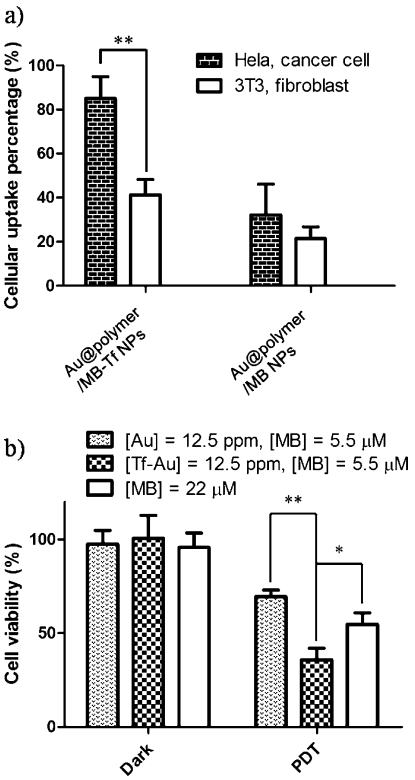

Figure 5. (a) A cellular uptake examination of Au@polymer-Tf NPs and Au@polymer NPs was conducted on HeLa cells and 3T3 fibroblasts for 24 h. b) MTT assay for Au@polymer/MB NPs-, Au@polymer/MB-Tf NPs-, and free MB-treated HeLa cells for 2 h, followed by replacing the particle-containing media. The sample-treated cells were reacted under two conditions of 660 nm light excitation for 4 min and dark aging (4 min), followed by a further incubation for 24 h. [Au] represents the concentration of the Au@polymer NPs in a cell culture medium, whereas [MB] represents the final concentration of MB in the cell culture medium. All data are presented as mean ± standard deviation (n = 3).

accumulation of the sample dose was approximately 3 times higher for the Au@polymer-Tf NPs to HeLa cells than the percentage of the Au@polymer NPs. This result is similar to the study of Parab et al., who used J5 liver cancer cells.[39] It should be noted that the uptake percentage in the 3T3 cells also increased with the Au@polymer-Tf NPs. In spite of this fact, the cellular uptake percentage of the Au@polymer-Tf NPs in HeLa cells was almost 2-fold higher than in 3T3 cells. When compared to the result reported by Song et al. that showed that folic acid could enhance cellular uptake in HeLa cells to 1.5-fold higher than 3T3 fibroblasts,[40] transferrin also appeared to be a good ligand candidate for cancer targeting therapy. This result indicates that the cancer cell targeting selectivity of Au@polymer nanocarriers is significantly enhanced after Tf modification, which might be followed with a transferrin receptor-mediated endocytosis pathway.[38]

dx.doi.org/10.1021/am5064298 | ACS Appl. Mater. Interfaces XXXX, XXX, XXX−XXX

2.7. PDT Efficiency Using Au@polymer-Tf NPs. Au@polymer/MB-Tf NPs and Au@polymer/MB NPs containing culture media (12.5 $ppm_{[Au]}$ and 5.5 $\mu M_{[MB]}$) were utilized to coincubate HeLa cells for 2 h. Solution at 22 $\mu M_{[MB]}$ was prepared in a medium to treat cells (2 h) for a comparison. A fresh medium solution was employed to replace the reagents, including the medium, before 660 nm light and dark treatments. These cells were cultured again for another 24 h. No groups had significant dark toxicity because they were incubated for only 2 h (Figure 5b). Upon exposure to laser light (32 mW/cm^2) at 660 nm for 4 min, the Au@polymer/MB-Tf NPs had the highest PDT efficiency (~65% of cell death) compared to the Au@polymer/MB NPs (~45% of cell death) and the free MB group (~30% of cell death) with a 4-fold higher MB concentration. Combined with cellular interaction analysis (Figure 5a), a surface modification of Tf on the Au@polymer nanocarrier appears to successfully target cancer cells and thus significantly enhance, by over 2-fold, the PDT efficacy, over the use of free MB at 4 times dosage.

2.8. ROS Generation Monitoring: DCFH-DA Staining. To prove the ROS induced by Au@polymer/MB-Tf NPs for PDT treatment of cancer cells, in vitro ROS generation monitoring was conducted. To detect the generated ROS, 2′,7′-dichlorofluorescin diacetate (DCFH-DA) was used. Owing to its great permeability through cell membranes, it could easily enter into the cells and then be hydrolyzed into 2′,7′-dichlorodihydrofluorescein (DCFH) by cellular esterases.[41] Once the ROS was presented, DCFH would react with it to form 2′,7′-dichlorofluorescein (DCF), which fluoresces green (Figure 6a). After loading the DCFH-DA, the Au@polymer/MB-Tf NPs and Au@polymer/MB NPs containing culture media (12.5 $ppm_{[Au]}$ and 5.5 $\mu M_{[MB]}$) were incubated with HeLa cells for 2 h, followed by irradiation for 4 min. After the PDT treatment, fluorescence images of DCF (green) were taken and are shown in Figure 6b. Stronger green fluorescence of DCF was observed in Au@polymer/MB-Tf NPs and Au@polymer/MB NPs as compared to that of free MB. There was very weak fluorescence in the control group. To semiquantify the DCF signals in the cells, ImageJ was used to analyze the ROS generation in cells by measuring the integrated fluorescence intensity per area of the fluorescence image. The results are shown in Figure 6c. In comparison to the free MB and control results, higher ROS levels were reported when using Au@polymer/MB NPs. This implied the success of Au@polymer NP carried MB for enhancing the PDT efficiency. With the aid of transferrin, the Au@polymer/MB-Tf NPs induced the highest ROS level of all the groups, indicating a further enhancement in the PDT efficacy.

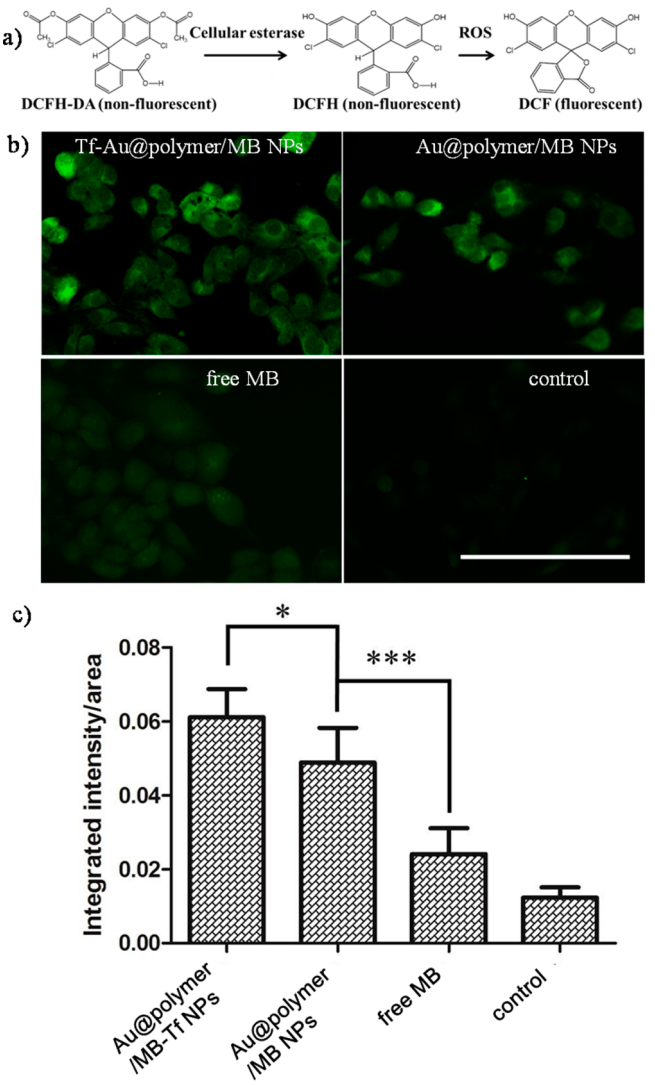

Figure 6. Intracellular ROS generation for PDT treatment in vitro with DCFH-DA: (a) schematic representation for the conversion of the DCFH-DA to generate green fluorescent DCF molecule by reacting with ROS species, (b) fluorescence images of DCF (green) in HeLa cells incubated with Au@polymer-Tf NPs and Au@polymer/MB NPs and pure MB after receiving 660 nm laser exposure for 4 min (scale bar: 100 μm). (c) Integrated fluorescence intensity per area in each group. *, $P < 0.05$, data are presented as mean ± standard deviation.

2.9. Annexin V-FITC/PI Staining. Because ROS is essential in several vital regulatory pathways, the ROS levels in cells are kept in balance under normal conditions. An excessive ROS level could be fatal, owing to its character in activating cell-cycle inhibitors and triggering cell death pathways at high levels.[42,43] To verify the cell death pathway, Annexin V-FITC and PI dyes were applied to stain the inversion of phosphatidylserine with green fluorescence and binding into DNA with red fluorescence.[44] Au@polymer/MB and Au@polymer/MB-Tf NPs (12.5 $ppm_{[Au]}$ and 5.5 $\mu M_{[MB]}$) containing culture media were incubated with HeLa cells for 2 h, followed by fresh medium replacement and a 660 nm light treatment. An MB group at a concentration of 5.5 μM was also used. At 4 h/24 h post irradiation time, each group was stained with Annexin V-FITC (green)/PI(red) dyes and monitored by using fluorescence microscopy. The resulting fluorescence images are shown in Figure 7. At 4 h after irradiation, green fluorescence signals of Annexin V-FITC are seen in the Au@polymer/MB and Au@polymer/MB-Tf NPs and pure MB-treated groups (Figure 7a). A few red fluorescence spots of PI were detected. In the reagent-free treatment, as a control group, no obvious fluorescence signals were obtained for the cells. The Annexin V-FITC positive/PI negative cells imply that cell membrane inversion has occurred, which is a special characteristic of early stage apoptosis. At 24 h post 660 nm light treatment, the cell membranes of apoptotic cells have no integrity (Figure 7b), allowing the PI dye to enter the cell nuclei. Indeed, the red fluorescence of the PI could be observed in late-stage apoptotic cells. Double-positive stained cells were found in the Au@polymer/MB and Au@polymer/MB-Tf NPs

dx.doi.org/10.1021/am5064298 | ACS Appl. Mater. Interfaces XXXX, XXX, XXX−XXX

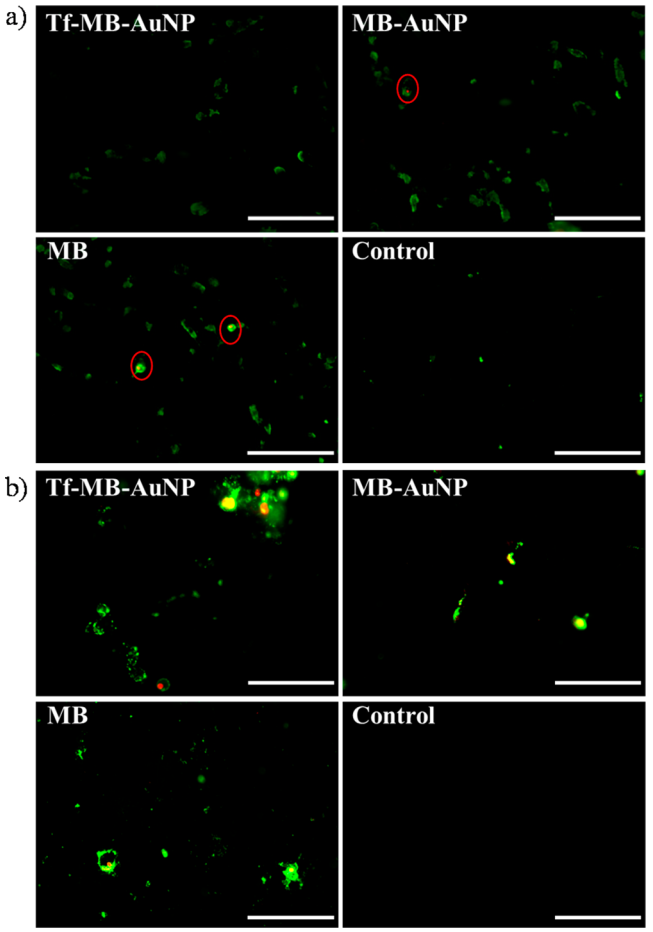

Figure 7. Fluorescence images of Annexin V-FITC (green) and PI (red) in HeLa cells incubated with Au@polymer/MB-Tf NPs and Au@polymer/MB NPs and free MB at (A) 4 h (B) 24 h postirradiation (a single 4 min hand-held 32 mW/cm^2 laser treatment) (scale bar: 100 μm).

and pure MB-treated groups, while no fluorescence was detected in the control group (Figure 7b).

Lu et al. reported that free MB PSs induced a series apoptotic process in HeLa cells upon excitation at 660 nm.[11] Dead cell bodies induced from apoptotic pathway are removed by phagocytosis without affecting neighboring healthy cells. However, necrosis is unfavorable for normal body tissue because it positively correlates with inflammatory diseases and metastasis.[44,45] On the basis of DCFH-DA (Figure 6) and Annexin V-FITC/PI (Figure 7c) staining, these images demonstrated that using Au@polymer/MB-Tf NPs treatment can cause an MB-dependent apoptotic cell death. However, the PDT effects of Au@polymer/MB-Tf NPs aid antitumor mechanism will need further justification through animal study.

3. CONCLUSION

We have developed a more effective but less harmful Au@polymer/MB-Tf NP, consisting of a sandwich structure with a Tf coating at the uppermost surface, a polymer/MB intermediate layer, and an Au interior nanocore as a new nano-object photosensitizer for PDT treatment. MB PSs absorbed on the Au@polymer NPs were examined to improve the dark toxicity due to a strong absorption interaction, thereby preventing the MB from leaking out. Fluorescence examinations established an emission peak at ~1270 nm from a 660 nm light excitation of Au@polymer/MB NPs, suggesting a correlation of the generation of type II phototoxicity ($^1O_2$) with a quantum yield comparable to that of free MB PS. In vitro studies showed that the Au@polymer/MB-Tf NPs produced more ROS than MB alone in the cellular environment due to the locally concentrated effect, resulting in a superior PDT efficacy for killing HeLa cells via the apoptotic pathway.

It is worthy of mention that the Au NPs provided additional features as multifunctional nanoagents for molecular contrast enhancement in modern molecular imaging, such as multiphoton imaging, SRES tag for tracking, computed tomography (CT) enhancement, and photoacoustic imaging.[15,28] Combined with these imaging abilities, Au@polymer/MB-Tf NPs could act as tumor tracers, which offer a potent development for an imaging-guided therapeutic platform.

4. EXPERIMENTAL SECTION

4.1. Materials. Hydrogen tetrachloroaurate(III) trihydrate ($HAuCl_4 \cdot 3H_2O$) (Alfa-Aesar 36400), methylene blue (Alfa-Aesar A18174), poly(styrene-*alt*-maleic acid) sodium salt solution (PSMA) (Aldrich 662631), blue tetrazolium bromide (MTT reagent) (Alfa-Aesar L11939), dimethyl sulfoxide (DMSO) (Scharlau SU0155), Dulbecco's Modification of Eagle's medium—high glucose (DMEM-HG) (Thermo Hyclon SH30003.02), phosphate buffered saline (PBS) tablet (Sigma P4417), fetal bovine serum (FBS) (Biological 04-001-1A), antibiotic antimycotic solution (Penicillin/Streptomycin/Amphotericinβ) (Biological 03-033-1B), trypsin-EDTA (Biological 03-051-5B), 9,10-anthracenediyl-bis(methylene)dimalonic acid (ABDA) (FLUKA 75068), apo-transferrin human (Tf) (Sigma-Aldrich T5391), 4-morpholineethanesulfonic acid (MES) hydrate (Sigma M2933), *N*-(3-(dimethylamino)propyl)-*N*′-ethylcarbodiimide hydrochloride (EDC) (Fluka 03450), *N*-hydroxysuccinimide (NHS) (Aldrich 130672), quantiPro BCA Assay kit (Sigma QPBCA), sodium hydroxide (Mallinckrodt 7708—100), hydrochloric acid (Fish Scientific 231-595-7), 2′,7′-dichlorofluorescin diacetate (DCFH-DA) (Sigma-aldrich D6883), annexin V-FITC fluorescence microscopy kit (BD Pharmingen 550911), propidium iodide staining solution (BD Pharmingen 556463). All chemicals were used as received.

4.2. Synthesis of Au@polymer NPs. Au@polymer core—shell NPs were synthesized according to the one-pot synthesis method that we have developed.[15] Initially, 1 mL of $HAuCl_4$ (5 mM), 7.5 mL of DI water, and 2.5 mL of poly(styrene-*alt*-maleic acid) sodium salt (PSMA) solution (24 mg/mL) were introduced into a 23 mL Teflon-lined stainless steel autoclave. The reactor was kept in a circulator oven (DENG YNG) at 200 °C. After 6 h, the redox reaction was completed. The solution was centrifuged at 11000 rpm for 10 min. The supernatant was removed, and the pellet was resuspended with 4 mL of DI water. The solution was centrifuged again at 11000 rpm for 10 min, and the supernatant was removed before the pellet was resuspended with DI water. The final concentration of Au NPs was adjusted to 500 $ppm_{[Au]}$ for further use, based on the atomic absorption spectroscopy measurements.

4.3. Preparation of Au@polymer/MB NPs. Au@polymer/MB NPs were prepared by setting up several groups of solutions containing 0.1 mL of AuNP solution (~550 ppm), 1 mL of DI water, and 0/4/8/12/24/48/80 μL of MB (0.5 mM). Each group was kept at room temperature and in the dark. After the solution was mixed overnight during the MB adsorption, the products were purified by centrifugation and redispersion processes. UV—visible measurements indicated that no detectable absorption signals were obtained from the first supernatant of the loading of 0—48 μL of MB (0.5 mM). Subsequently, each group was redispersed in 1.1 mL of H_2O solution. The final concentration of [Au] was ~50 ppm, and the concentration of MB in each group was estimated to be ~0/1.8/3.6/5.5/11/22 μM, respectively. Control groups containing pure MB with the same concentrations as above were also prepared.

4.4. Optical Characterization of Au@polymer/MB NPs. To observe the optical behaviors of the Au@polymer/MB NPs that were

dx.doi.org/10.1021/am5064298 | ACS Appl. Mater. Interfaces XXXX, XXX, XXX—XXX

prepared at different concentrations, we centrifuged the solutions of each group at 11000 rpm for 10 min to separate the nonadsorbed MB. The supernatants were collected, and the pellet was resuspended in 1 mL of DI water. The collected supernatants containing the nonadsorbed MB were centrifuged again at 13000 rpm for 20 min to remove the remaining Au@polymer NPs, after which the supernatants were collected again. The UV−visible absorption spectra of each group were recorded by a UV−visible spectrometer. The loading amount of MB on the Au@polymer NPs was determined by using Lambert−Beer's Law to compare the absorbance at a wavelength of 660 nm for each collected supernatant and corresponding control group.

In a saturation absorption condition through a complete reaction of ∼50 $ppm_{[Au]}$ Au@polymer NPs solution with a 22 μM MB concentration, the loading amount of MB on the Au@polymer NPs was calculated to be 0.0024 μmol. The total amount of the Au@polymer NPs in this solution was measured to be 8.138×10^{-14} mole by assuming uniform spherical morphology with a mean diameter of 21.46 nm and a density of 19.3 g/cm^3. Thus, it can be estimated that an average of 29 490 MB molecules was attached on a single Au@polymer NP.

4.5. Stability Tests of the Au@polymer/MB NPs. An Au@polymer/MB NPs solution at 22 μM of MB concentration (∼50 $ppm_{[Au]}$) was used in this test. The solution was kept at room temperature and in the dark. We centrifuged the solution (0.1 mL) at 11000 rpm for 10 min. The supernatants that contained the released MB were collected after 1/4/7/14 days. The UV−visible absorption spectra of the supernatant at each time point were recorded using a UV−visible spectrometer. The amount of MB leaking out of the Au@polymer/MB NPs was quantified using the Beer−Lambert Law. Fresh Au@polymer/MB NPs were also prepared after centrifugation and were resuspended in 0.1 mL of DI water and phosphate buffered saline (PBS). After 1/4/7/14 days of incubation time, the as-obtained samples were characterized with a UV−visible spectrometer.

4.6. ROS Generation Test: ABDA Method. Initially, 0.2 mg ABDA was dispersed in 0.1 mL dimethyl sulfoxide (DMSO). Next, ABDA solution was diluted with DI water, followed by mixing with different doses of samples. Final concentrations of ABDA in each group were 0.1 mg/mL reacted with ∼50 $ppm_{[Au]}$ of Au@polymer/MB NPs including [MB] concentrations at 11 μM and 22 μM. To verify the effect of [Au] on ROS generation, the two above groups were diluted 4-fold to prepare a 12.5 $ppm_{[Au]}$ of Au@polymer/MB NPs solution including MB concentrations at 2.7 and 5.5 μM. Free MB groups that contained pure MB with the same above concentrations were also prepared. A 96-well plate was used with each well containing 0.2 mL solution of each group, followed by an exposure to a 660 nm laser (75 mW) for 4/10/20/30 min, respectively. Then absorbance at a wavelength of 380 nm at different time points was recorded by a microplate reader (Awareness Technology). The whole process was done without light exposure.

4.7. Cell Culture. 3T3 fibroblast cells (National Taiwan University, Department of Medical Engineering) and HeLa cells (National Taiwan University, Department of Plant Pathology and Microbiology) were cultured in DMEM-HG culture medium. Cell culture began with a cell seeding density of about 3×10^4 cells/cm^2 on a 10 cm culture dish at 37 °C, 5% CO_2. After confluency was reached, the cells were cultured with trypsin-EDTA for 4 min at 37 °C to detach the cells from the culture dish. To stop the enzyme reaction, culture medium was added to the dish. The suspended cells were counted using a hemocytometer; cells were stained with trypan blue to test cell viability. After trypsinization, the cells were collected for further experiments.

4.8. In Vitro Cell Toxicity Test. We tested cell viability with Au@polymer/MB NPs seeding HeLa cells at a density of 5000 per well in a 96-well plate. After 1 day of incubation, we dispersed the Au@polymer/MB NPs (11 and 22 μM of [MB] adsorbed) in culture media and then added 100 μL (∼50 $ppm_{[Au]}$) to each well to replace the original culture medium. Approximately 12.5 $ppm_{[Au]}$ of Au@polymer/MB NPs, including 2.7 $\mu M_{[MB]}$ and 5.5 $\mu M_{[MB]}$, were prepared by diluting the above particle samples four times in a parallel experiment. As a control, we used an MB containing medium with the same concentration. In the PDT treatment, after individual samples were introduced for 2 h, we applied a 660 nm light (32 mW/cm^2) to each well for 4 min, containing the original media without a fresh medium as a substitute. The PDT-treated cells were then kept in the incubator for 1 day, again followed by an MTT assay. In the dark toxicity group (without laser treatment), the particle-treated cells were kept in an incubator for 1 day followed by an MTT assay. Cell viability was reported as a percentage, a ratio between the treated groups and the control group (without particle and laser treatment).

To understand the cell specificity, we carried out HeLa, A549 cell (human lung adenocarcinoma epithelial cell line), and HT1080 cell (fibrosarcoma cell line) incubated with Au@polymer/MB NPs (12.5 $ppm_{[Au]}$ and 5.5 $\mu M_{[MB]}$) and free MB (5.5 $\mu M_{[MB]}$) for 2 h. Next, PDT (exposure to a 660 nm light for 4 min) treatment was applied. The cell viability was determined by utilizing the MTT assay.

4.9. Transferrin Grafting on Au@polymer NPs. To bind transferrin (Tf) on Au@polymer NPs, we diluted AuNP solution (∼500 ppm) 10-fold in 0.45 mL of MES buffer (100 mM, pH= 5.5) to activate the carboxylate groups at the PSMA structure. Subsequently, 10 μL of *N*-(3-(dimethylamino)propyl)-*N*′-ethylcarbodiimide hydrochloride (EDC, 100 mM) and 25 μL of *N*-hydroxysuccinimide (NHS, 100 mM) solutions were added to the solution. After 30 min, the activated Au@polymer NP solution was centrifuged at 13000 rpm for 20 min at 4 °C to remove excess EDC/NHS and the particles were resuspended in 0.5 mL of PBS. Finally, the Au@polymer NP solution was mixed with 0.5 mL of the apo-transferrin human solution (60 μg/mL) for a substitution reaction overnight at room temperature.[35] The particles were then separated from the excess Tf by centrifugation at 13000 rpm for 20 min at 4 °C and resuspended in 0.5 mL of DI water as a Au@polymer-Tf NP solution (∼50 ppm). The supernatant that contained excess Tf was collected. The nonconjugated material in the supernatant was quantified by a BCA assay (Figure S2, Supporting Information). The amount of the grafted transferrin was then determined.

4.10. Cellular Uptake Quantification. To compare the cell targeting selectivity between cancer cells and nonmalignant cells, HeLa cells and 3T3 fibroblasts (p13) were chosen for our work. HeLa cells/3T3 fibroblasts were seeded at a seeding density of 5000 per well in a 96-well plate. After the plate was cultured for 1 day, we dispersed the Au@polymer-Tf NPs/Au@polymer NPs in culture mediums (∼12.5 ppm) and then added 100 μL to each well to replace the original medium. After the particles were introduced for 2 h, each well was washed twice with PBS to remove the free particles. Subsequently, 150 μL of DMSO was introduced to each well to lyse the cells and to release the particles uptaken by the cells. The solution was collected and 70 μL of the solution was be mixed with 130 μL NaOH solution (8 mM) to dissolve the PSMA layer of the particle. After 1 h, 1.8 mL of 4.5 M HCl solution was applied to digest the particles into smaller sizes for further measurement. Finally, the cellular uptake amount was quantified by an atomic analyzer (AA, PerkinElmer). To normalize the slight difference between concentrations of Au@polymer-Tf NPs and Au@polymer NPs, cellular uptake amounts were divided by the amount we initially introduced in the culture medium and reported as a percentage.

4.11. Intracellular ROS Generation Monitoring: DCFH-DA staining. To detect ROS generation in vitro, we prepared 10 mM 2′,7′-dichlorofluorescin diacetate (DCFH-DA) solution in DMSO and diluted it 10-fold with PBS buffer as 1 mM stock. Next, a DCFH-DA stock solution was mixed with PBS at a ratio of 2:98 as a working solution (20 μM) for further use. We cultured HeLa cells at a seeding density of 50 000 cells (1 mL) in one well (10.7 × 9.4 mm) of the chamber slide for 1 day. The cells were incubated with 1 mL of working solution for 30 min for DCFH-DA uptake and then washed once with PBS to remove excess DCFH-DA. After the DCFH-DA loading, 1 mL of Au@polymer/MB NPs and Au@polymer/MB-Tf NPs containing medium (∼12.5 ppm [Au] and 5.5 $\mu M_{[MB]}$) was added. A free MB-containing medium at 5.5 μM was also used as a control. After 2 h of incubation, the particle containing medium was removed, and the slide was washed and rinsed with PBS. Each group

received PDT (by applying a 660 nm laser for 4 min) and was monitored by a fluorescence microscope (Nikon) to detect ROS generation. The intensity of fluorescence staining on intracellular ROS was analyzed with ImageJ 1.48 software. The integrated green fluorescence in each sample was available after deducting by background fluorescence from the background. The integrated fluorescence intensity was calculated based on 50 cells.

4.12. Cancer Cell Targeting Effect on PDT. Similar to the in vitro cell toxicity test, we tested cell viability with Au@polymer-Tf NPs and MB NPs/Au@polymer/MB NPs by using HeLa cells. Au@polymer/MB-Tf NPs and Au@polymer/MB NPs were added into culture media (12.5 $ppm_{[Au]}$ and 5.5 $\mu M_{[MB]}$). A medium group containing only MB (22 μM) was also used as a control. Next, 100 μL of the particle containing medium was added to each well. To verify the influence of the transferrin conjugation on the therapeutic efficiency, we replaced the particle containing medium with a fresh one after the particles were incubated with the cells for 2 h. PDT (applied by a 660 nm laser for 4 min)/dark (without laser application) treatments were carried out. After 1 day of incubation, the cell viability was measured by an MTT assay. Cell viability was reported as a percentage calculated as a ratio between the treated groups and the control group (without particles and laser treatment).

4.13. Annexin V-FITC/PI Staining. HeLa cells incubated with Au@polymer/MB-Tf NPs and Au@polymer/MB NPs underwent PDT treatment and were monitored. We cultured HeLa cells at a seeding density of 50 000 per mL on a microscope slide (total 1 mL) for 1 day. These cells were then incubated with the particles. After 2 h of incubation with 1 mL of Au@polymer/MB-Tf NPs and the Au@polymer/MB NPs containing medium (~12.5 ppm $_{[Au]}$ and 5.5 μM of [MB] adsorbed), the medium was replaced with fresh media. The medium group containing only MB (5.5 μM) was also used as a control. Next, PDT (exposure to a 660 nm laser for 4 min) treatment was applied. To detect early stage apoptosis and necrosis, all cells were stained by Annexin V−fluorescein isothiocyanate (Annexin V-FITC)/propidium iodide (PI) for 15 min. Fluorescence images of HeLa cells at 4 and 24 h post-treatment were taken by a fluorescence microscope (Nikon). For these cells, membrane inversion was detected by Annexin V-FITC (green) and the subsequent membrane rupture was verified by PI (red).[11]

4.14. Characterization. The structure and optical property of Au@polymer NPs were characterized by transmission electron microscopy (TEM, JEOL), multipurpose X-ray thin-film diffractometer (XRD, Rigaku), UV−vis spectrophotometer (8452A; Hewlett-Packard Company, Palo Alto, CA), and zetasizer analyzer (Malvern Instruments, Malvern, UK).

4.15. Statistical Analysis. All data are expressed as means ± standard deviation. Comparison of different groups was determined using Student's *t*-test and significant difference was assumed at *P*-value ≤0.05. The statistical data was analyzed using SigmaPlot 10.0 (Systat Software, San Jose, CA).

■ ASSOCIATED CONTENT

Ⓢ Supporting Information

Table for the ζ-potential measurements of Au@polymer NPs, UV−visible spectra records of a loading amount of MB molecules on Au@polymer NPs, TEM image and UV−visible spectrum of Au@polymer NPs reacted with 36 μM of MB molecule, photostability of free MB and Au@polymer/MB NPs, the release of MB from Au@polymer/MB NPs, MTT assay for cell specificity, BCA assay at 570 nm for the conjugation of Tf on a single Au@polymer NP, and UV/visible spectra of Au@polymer-Tf NPs and Au@polymer/MB-Tf. This material is available free of charge via the Internet at http://pubs.acs.org.

■ AUTHOR INFORMATION

Corresponding Authors

*Prof. Jiashing Yu. E-mail: jiayu@ntu.edu.tw.

*Prof. Chih-Chia Huang. E-mail: cchuang-ym@ym.edu.tw; huang.chihchia@gmail.com.

Author Contributions

⊥These authors contributed equally.

Notes

The authors declare no competing financial interest.

■ ACKNOWLEDGMENTS

This work was supported by the Ministry of Science and Technology, Taiwan (MOST 103-2113-M-010-001-MY2, MOST-102-2221-E-002-039, NSC 102-2221-E-010-006-MY3, and NSC 101-2113-M-010-002-MY2).

■ REFERENCES

(1) Moskal, T. L.; Dougherty, T. J.; Urschel, J. D.; Antkowiak, J. G.; Regal, A. M.; Driscoll, D. L.; Takita, H. Operation and Photodynamic Therapy for Pleural Mesothelioma: 6-year Follow-up. *Ann. Thorac. Surg.* **1998**, *66*, 1128−1133.

(2) Duncan, R.; Sat, Y. N. Tumour Targeting by Enhanced Permeability and Retention (EPR) Effect. *Ann. Oncol.* **1998**, *9*, 39−39.

(3) Dougherty, T. J.; Gomer, C. J.; Henderson, B. W.; Jori, G.; Kessel, D.; Korbelik, M.; Moan, J.; Peng, Q. Photodynamic Therapy. *J. Natl. Cancer Inst.* **1998**, *90*, 889−905.

(4) Tardivo, J. P.; Del Giglio, A.; de Oliveira, C. S.; Gabrielli, D. S.; Junqueira, H. C.; Tada, D. B.; Severino, D.; de Fátima Turchiello, R.; Baptista, M. S. Methylene Blue in Photodynamic Therapy: From Basic Mechanisms to Clinical Applications. *Photodiagn. Photodyn. Ther.* **2005**, *2*, 175−191.

(5) Tuite, E. M.; Kelly, J. M. Photochemical Interactions of Methylene Blue and Analogues with DNA and Other Biological Substrates. *J. Photochem. Photobiol., B* **1993**, *21*, 103−124.

(6) Gabrielli, D.; Belisle, E.; Severino, D.; Kowaltowski, A. J.; Baptista, M. S. Binding, Aggregation and Photochemical Properties of Methylene Blue in Mitochondrial Suspensions. *Photochem. Photobiol.* **2004**, *79*, 227−232.

(7) Peng, Q.; Berg, K.; Moan, J.; Kongshaug, M.; Nesland, J. M. 5-Aminolevulinic Acid-based Photodynamic Therapy: Principles and Experimental Research. *Photochem. Photobiol.* **1997**, *65*, 235−251.

(8) Salva, K. A. Photodynamic Therapy: Unapproved Uses, Dosages, or Indications. *Clin. Dermatol.* **2002**, *20*, 571−581.

(9) Konig, K. Multiphoton Microscopy in Life Sciences. *J. Microsc.* **2000**, *200*, 83−104.

(10) Tian, G.; Gu, Z.; Zhou, L.; Yin, W.; Liu, X.; Yan, L.; Jin, S.; Ren, W.; Xing, G.; Li, S.; Zhao, Y. Mn^{2+} Dopant-Controlled Synthesis of NaYF4:Yb/Er Upconversion Nanoparticles for in Vivo Imaging and Drug Delivery. *Adv. Mater.* **2012**, *24*, 1226−1231.

(11) Lu, Y.; Jiao, R. Q.; Chen, X. P.; Zhong, J. Y.; Ji, A. G.; Shen, P. P. Methylene Blue-Mediated Photodynamic Therapy Induces Mitochondria-Dependent Apoptosis in HeLa Cell. *J. Cell. Biochem.* **2008**, *105*, 1451−1460.

(12) Zhang, L. Z.; Tang, G. Q. The Binding Properties of Photosensitizer Methylene Blue to Herring Sperm DNA: A Spectroscopic Study. *J. Photochem. Photobiol., B* **2004**, *74*, 119−125.

(13) Yao, J.; Zhang, G. J. Loss of Lysosomal Integrity Caused by the Decrease of Proton Translocation in Methylene Blue-Mediated Photosensitization. *Biochim. Biophys. Acta* **1996**, *1284*, 35−40.

(14) Kanduc, D.; Mittelman, A.; Serpico, R.; Sinigaglia, E.; Sinha, A. A.; Natale, C.; Santacroce, R.; Di Corcia, M. G.; Lucchese, A.; Dini, L.; Pani, P.; Santacroce, S.; Simone, S.; Bucci, R.; Farber, E. Cell Death: Apoptosis versus Necrosis (Review). *Int. J. Oncol.* **2002**, *21*, 165−170.

(15) Liu, T. M.; Yu, J.; Chang, C. A.; Chiou, A.; Chiang, H. K.; Chuang, Y. C.; Wu, C. H.; Hsu, C. H.; Chen, P. A.; Huang, C. C. One-Step Shell Polymerization of Inorganic Nanoparticles and Their Applications in SERS/Nonlinear Optical Imaging, Drug Delivery, and Catalysis. *Sci. Rep.* **2014**, *4*, 5593.

(16) Jiang, W.; Kim, B. Y.; Rutka, J. T.; Chan, W. C. Nanoparticle-mediated Cellular Response is Size-Dependent. *Nat. Nanotechnol.* **2008**, *3*, 145−150.
(17) Asati, A.; Santra, S.; Kaittanis, C.; Perez, J. M. Surface-Charge-Dependent Cell Localization and Cytotoxicity of Cerium Oxide Nanoparticles. *ACS Nano* **2010**, *4*, 5321−5331.
(18) El-Sayed, I. H.; Huang, X.; El-Sayed, M. A. Surface Plasmon Resonance Scattering and Absorption of Anti-EGFR Antibody Conjugated Gold Nanoparticles in Cancer Diagnostics: Applications in Oral Cancer. *Nano Lett.* **2005**, *5*, 829−834.
(19) Liu, X.; Chen, Y.; Li, H.; Huang, N.; Jin, Q.; Ren, K.; Ji, J. Enhanced Retention and Cellular Uptake of Nanoparticles in Tumors by Controlling Their Aggregation Behavior. *ACS Nano* **2013**, *7*, 6244−6257.
(20) Zhang, S.; Li, J.; Lykotrafitis, G.; Bao, G.; Suresh, S. Size-Dependent Endocytosis of Nanoparticles. *Adv. Mater.* **2009**, *21*, 419−424.
(21) Kanazawa, T.; Takashima, Y.; Murakoshi, M.; Nakai, Y.; Okada, H. Enhancement of Gene Transfection into Human Dendritic Cells Using Cationic PLGA Nanospheres with a Synthesized Nuclear Localization Signal. *Int. J. Pharm.* **2009**, *379*, 187−195.
(22) Jaiswal, J. K.; Mattoussi, H.; Mauro, J. M.; Simon, S. M. Long-Term Multiple Color Imaging of Live Cells Using Quantum Dot Bioconjugates. *Nat. Biotechnol.* **2003**, *21*, 47−51.
(23) Lewin, M.; Carlesso, N.; Tung, C. H.; Tang, X. W.; Cory, D.; Scadden, D. T.; Weissleder, R. Tat Peptide-Derivatized Magnetic Nanoparticles Allow in Vivo Tracking and Recovery of Progenitor Cells. *Nat. Biotechnol.* **2000**, *18*, 410−414.
(24) Josephson, L.; Tung, C. H.; Moore, A.; Weissleder, R. High-Efficiency Intracellular Magnetic Labeling with Novel Superparamagnetic-Tat Peptide Conjugates. *Bioconjugate Chem.* **1999**, *10*, 186−191.
(25) Yeh, Y. C.; Creran, B.; Rotello, V. M. Gold Nanoparticles: Preparation, Properties, and Applications in Bionanotechnology. *Nanoscale* **2012**, *4*, 1871−1880.
(26) Wang, C.; Ma, Z.; Wang, T.; Su, Z. Synthesis, Assembly, and Biofunctionalization of Silica-Coated Gold Nanorods for Colorimetric Biosensing. *Adv. Funct. Mater.* **2006**, *16*, 1673−1678.
(27) Kojic, N.; Pritchard, E. M.; Tao, H.; Brenckle, M. A.; Mondia, J. P.; Panilaitis, B.; Omenetto, F.; Kaplan, D. L. Focal Infection Treatment Using Laser-Mediated Heating of Injectable Silk Hydrogels with Gold Nanoparticles. *Adv. Funct. Mater.* **2012**, *22*, 3793−3798.
(28) Ahn, S.; Seo, E.; Kim, K.; Lee, S. J. Controlled Cellular Uptake and Drug Efficacy of Nanotherapeutics. *Sci. Rep.* **2013**, *3*, 1997.
(29) Tan, Y. N.; Su, X.; Zhu, Y.; Lee, J. Y. Sensing of Transcription Factor through Controlled-Assembly of Metal Nanoparticles Modified with Segmented DNA Elements. *ACS Nano* **2010**, *4*, 5101−5110.
(30) Tognalli, N. G.; Fainstein, A.; Vericat, C.; Vela, M. E.; Salvarezza, R. C. Exploring Three-Dimensional Nanosystems with Raman Spectroscopy: Methylene Blue Adsorbed on Thiol and Sulfur Monolayers on Gold. *J. Phys. Chem. B* **2005**, *110*, 354−360.
(31) Suvith, V. S.; Philip, D. Catalytic Degradation of Methylene Blue Using Biosynthesized Gold and Silver Nanoparticles. *Spectrochim. Acta, Part A* **2014**, *118*, 526−532.
(32) Khan, S.; Alam, F.; Azam, A.; Khan, A. U. Gold Nanoparticles Enhance Methylene Blue-Induced Photodynamic Therapy: A Novel Therapeutic Approach to Inhibit *Candida albicans* Biofilm. *Int. J. Nanomed.* **2012**, *7*, 3245−3257.
(33) Srivatsan, A.; Jenkins, S. V.; Jeon, M.; Wu, Z.; Kim, C.; Chen, J.; Pandey, R. K. Gold Nanocage-Photosensitizer Conjugates for Dual-Modal Image-Guided Enhanced Photodynamic Therapy. *Theranostics* **2014**, *4*, 163−174.
(34) Lovell, J. F.; Liu, T. W.; Chen, J.; Zheng, G. Activatable Photosensitizers for Imaging and Therapy. *Chem. Rev.* **2010**, *110*, 2839−2857.
(35) Shrivastava, R.; Jain, B.; Das, K. Spectroscopic Investigations on the Binding of Methylene Blue and Nile Blue to Negatively Charged Gold Nanorods. *J. Mol. Struct.* **2012**, *1020*, 56−62.
(36) Dickinson, B. C.; Chang, C. J. Chemistry and Biology of Reactive Oxygen Species in Signaling or Stress Responses. *Nat. Chem. Biol.* **2011**, *7*, 504−511.
(37) Zhao, T.; Wu, H.; Yao, S. Q.; Xu, Q. H.; Xu, G. Q. Nanocomposites Containing Gold Nanorods and Porphyrin-Doped Mesoporous Silica with Dual Capability of Two-Photon Imaging and Photosensitization. *Langmuir* **2010**, *26*, 14937−14942.
(38) Daniels, T. R.; Delgado, T.; Helguera, G.; Penichet, M. L. The Transferrin Receptor Part II: Targeted Delivery of Therapeutic Agents into Cancer Cells. *Clin. Immunol.* **2006**, *121*, 159−176.
(39) Parab, H. J.; Huang, J. H.; Lai, T. C.; Jan, Y. H.; Liu, R. S.; Wang, J. L.; Hsiao, M.; Chen, C. H.; Hwu, Y. K.; Tsai, D. P.; Chuang, S. Y.; Pang, J. H. Biocompatible Transferrin-Conjugated Sodium Hexametaphosphate-Stabilized Gold Nanoparticles: Synthesis, Characterization, Cytotoxicity and Cellular Uptake. *Nanotechnology* **2011**, *22*, 395706.
(40) Song, Y.; Chen, Y.; Feng, L.; Ren, J.; Qu, X. Selective and Quantitative Cancer Cell Detection Using Target-Directed Functionalized Graphene and Its Synergetic Peroxidase-like Activity. *Chem. Commun.* **2011**, *47*, 4436−4438.
(41) Curtin, J. F.; Donovan, M.; Cotter, T. G. Regulation and Measurement of Oxidative Stress in Apoptosis. *J. Immunol. Methods* **2002**, *265*, 49−72.
(42) Takahashi, A.; Ohtani, N.; Yamakoshi, K.; Iida, S.; Tahara, H.; Nakayama, K.; Nakayama, K. I.; Ide, T.; Saya, H.; Hara, E. Mitogenic Signalling and the p16INK4a-Rb Pathway Cooperate to Enforce Irreversible Cellular Senescence. *Nat. Cell Biol.* **2006**, *8*, 1291−1297.
(43) Ramsey, M. R.; Sharpless, N. E. ROS as a Tumour Suppressor? *Nat. Cell Biol.* **2006**, *8*, 1213−1215.
(44) Yoo, D.; Jeong, H.; Preihs, C.; Choi, J. S.; Shin, T. H.; Sessler, J. L.; Cheon, J. Double-Effector Nanoparticles: A Synergistic Approach to Apoptotic Hyperthermia. *Angew. Chem., Int. Ed.* **2012**, *51*, 12482−12485.
(45) Adams, R. M. Medicolegal Aspects of Occupational Skin Diseases. *Dermatol. Clin.* **1988**, *6*, 121−129.